SUPPORTING INFORMATION

Mixed anion control of negative thermal expansion in a niobium oxyfluoride

Eliza K. Dempsey[1] and James Cumby[1*]

[1] *School of Chemistry, University of Edinburgh, David Brewster Road, Edinburgh, EH9 3FJ.*

1 METHODS

1.1 Synthesis

NbO_2F and $NbO_{1.9}F_{1.1}$ samples were synthesised from stoichiometric quantites of Nb metal (99.8%, Alfa Aesar), Nb_2O_5 (99.99%, Merck Life Sciences) and NbF_5 (99%, Fluorochem) powders. A 9 mol % excess of NbF_5 was required to produce pure samples due to impurities or decomposition in the NbF_5. A presence of adsorbed water in the NbF_5 starting material is known to be an issue in the niobium oxyfluoride synthesis.[1, 2] Due to the moisture sensitive nature of NbF_5, all samples were weighed and ground in a glovebox under nitrogen. Samples were then placed in oxygen-free high conductivity (OFHC) copper ampoules (outside diameter: 9.5 mm, length: ~50 mm) under vacuum (~10^{-3} mbar) and sealed by cold-welding using a hydraulic pinch-off tool (Custom Products & Services Inc. HY-250). Due to a risk of high pressure forming within the copper ampoule due to NbF_5, some copper ampoules were also sealed in quartz ampoules under vacuum (~10^{-2} mbar). Samples were heated in a box furnace (heating rate: 10 ^{o}C min^{-1}) to 210^{o}C and held for 20 hours before being left in the furnace to cool to room temperature.

The higher fluorine content samples, x = 0.3-0.6, were synthesised from polytetrafluoroethylene (6-10 micron, Alfa Aesar), Nb metal (99.8%, Alfa Aesar) and Nb_2O_5 (99.99%, Merck Life Sciences) and weighed and ground under air. Samples were pelletised in a hydraulic press at a force of 2 tonnes and pellet diameter of 13 mm. The samples were then sealed in copper ampoules as described above. Due to the risk from high pressure forming from PTFE decomposition the copper ampoules were then also sealed in quartz ampoules under vacuum (~10^{-2} mbar). Samples were heated in a box furnace (heating rate: 1 ^{o}C min^{-1}) to 400^{o}C and held for 72 hours before being left in the furnace to cool to room temperature.

1.2 X-ray Powder Diffraction

Low temperature x-ray powder diffraction was performed using a Rigaku SmartLab XE with a copper sealed tube with a power of 40 kW. A Johannsson monochromoter produces $CuK\alpha_1$ (λ = 1.5401 Å) radiation. Measurements were performed in Bragg-Brentano geometry. A HyPix-300 detector was used. For the low temperature measurements the sample was held on a flat plate chromium-plated copper sample in an Oxford PheniX closed cycle helium cryostat. Data were collected whilst heating from 12 to 300 K in 5 K intervals allowing 15 minutes to equilibrate at each temperature. At each temperature, results were collected from 2θ = 20-120° with a 0.02° step size and a 0.34 seconds/step collection time. The higher fluorine content samples, x = 0.3-0.6, were found to decompose quickly in air and were therefore protected by kapton tape over the flat sample holder.

Additional measurements, including at high temperature, were carried out at the Swiss-Norwegian Beamline, BM01, at the European Synchrotron Radiation Facility. Samples were loaded into 0.3 mm quartz capillaries and sealed in a glovebox under Argon with measurements taken in transmission geometry. The PILATUS@SNBL diffractometer[3] was used with a wavelength of λ = 0.66627 Å and a sample to detector distance of 210 mm. Measurements were taken with a 2 second exposure time, for the x = 0.6 sample the capillary was rotated through 20^{o} during the measurement. Temperature was controlled using a Oxford Cryosystems 700 series cryostream cooler and a resistive capillary heater.[4] Scans were taken continuously

throughout heating and cooling. Patterns were integrated and processed using Bubble software developed by the beamline.

Pawley refinements to extract lattice parameters were performed using the GSAS-II software[5] and structure graphics generated using VESTA.[6] Full Rietveld refinements were performed for the high temperature synchrotron data to extract displacement parameters.

1.3 Magnetic Susceptibility

Magnetic susceptibility measurements were performed by vibrating sample magnetometry on a Quantum Design Physical Property Measurement system. Zero field cooled and field cooled measurements were taken from 4-300 K with an applied field of 2000 Oe. Moment against field measurements were also between -70000 to 70000 Oe. The samples were contained in the Quantum Design supplied powder sample holder secured with a small amount of vacuum grease. Magnetic susceptibility was fitted to a Curie-Weiss law (eq. 1) to extract a value for the Curie constant, C. The effective magnetic moment was then calculated allowing the oxidation state of niobium to be estimated assuming a spin only magnetic moment (eq. 2) where x corresponds to the composition $NbO_{2-x}F_{1+x}$.

$$\chi_m = \frac{C}{T - \theta_W} + \chi_0 \qquad (1)$$

$$\mu_{eff} = 2.828\sqrt{C} = \sqrt{3x} \qquad (2)$$

2 POWDER X-RAY DIFFRACTION

2.1 Rietveld Refinements

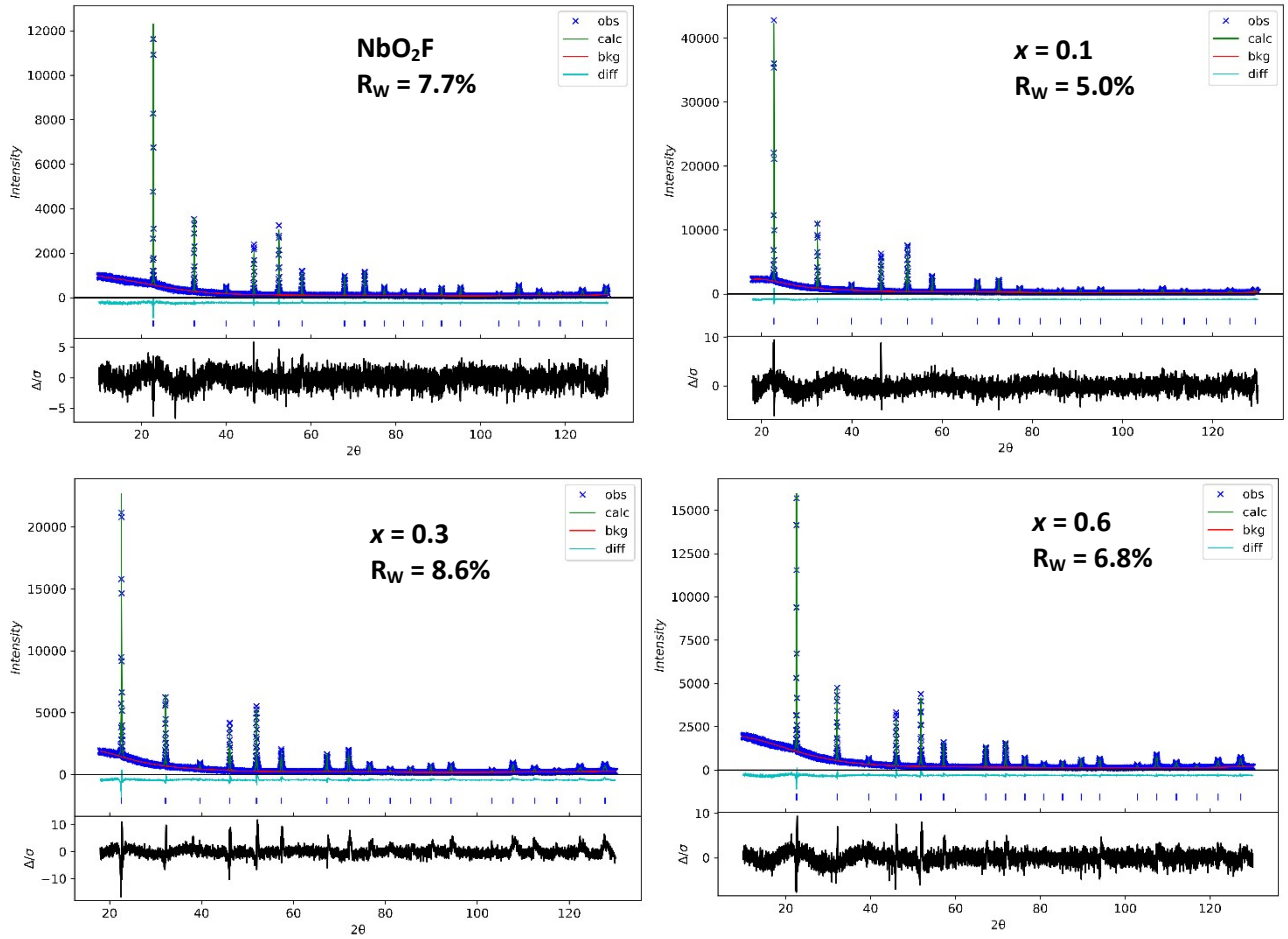

Fig. S2.1 Rietveld fitting to x-ray powder diffraction measurements on $NbO_{2-x}F_{1+x}$.

2.2 Ambient Lattice Parameters

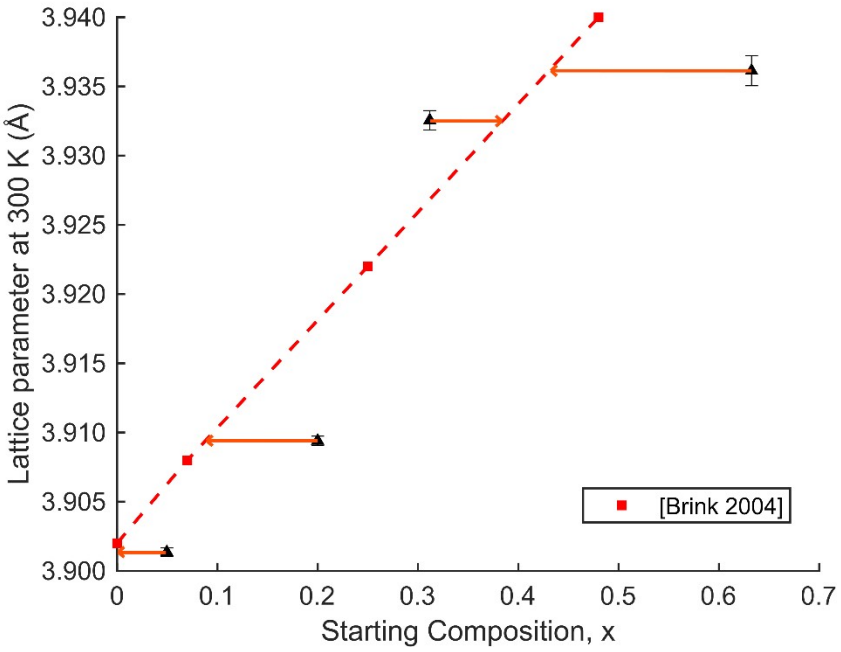

Fig. S2.2 Plot of measured lattice parameters against the starting synthesis composition of $NbO_{2-x}F_{1+x}$. Literature lattice parameter values from Brink *et al.* are also shown with composition corrected according to these values.[2]

2.3 Variation in Unit Cell Volume with Temperature

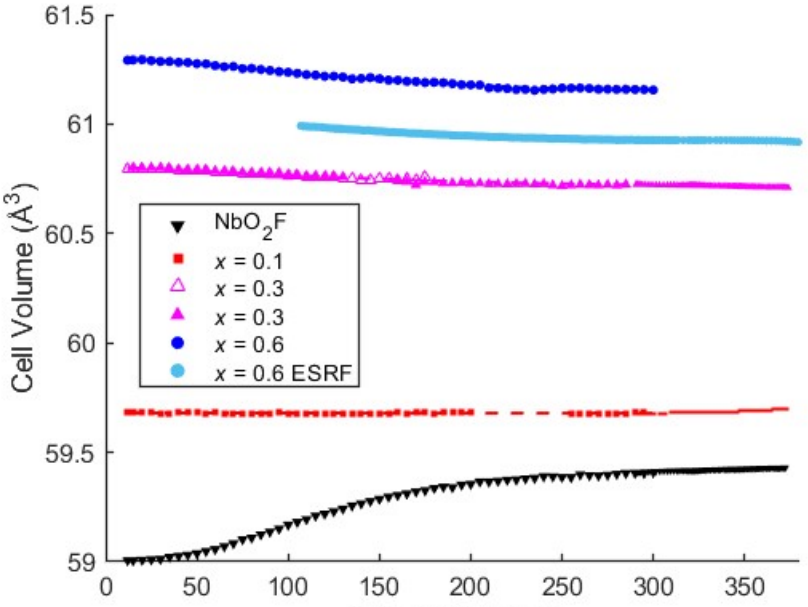

Fig. S2.3 Variation in absolute unit cell volume of $NbO_{2-x}F_{1+x}$ during heating.

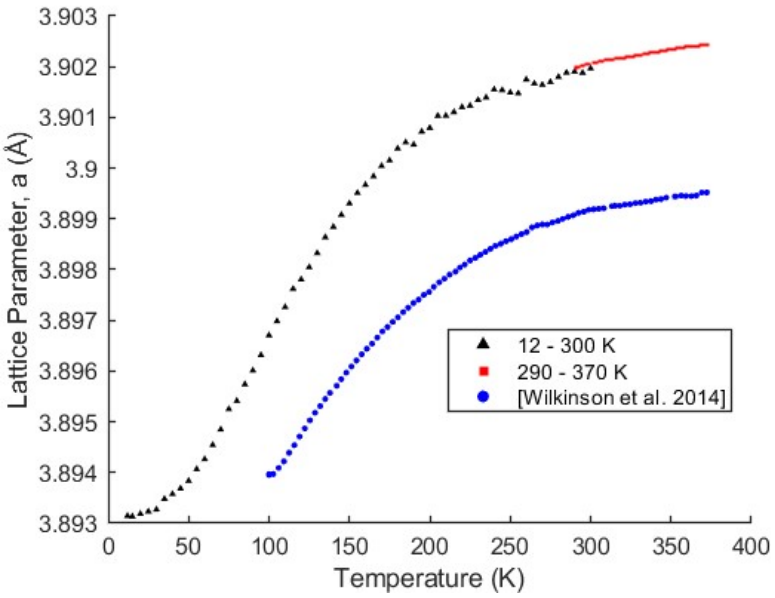

Fig. S2.4 Comparison of NbO_2F thermal expansion with previous published data from Wilkinson *et al.*[1]

2.4 Volumetric Coefficient of Thermal Expansion

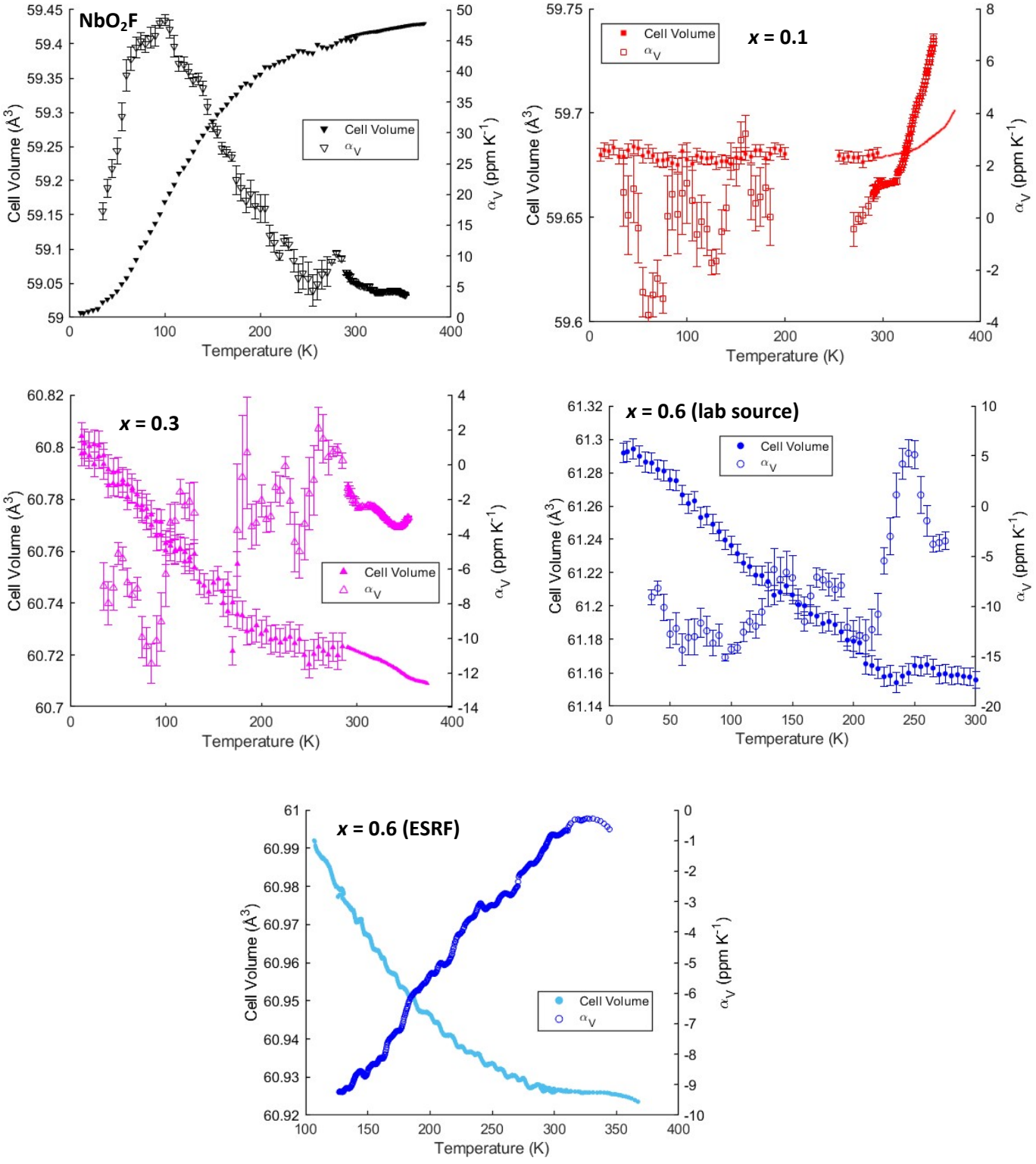

Fig. S2.5. Volumetric coefficients of thermal expansion for $NbO_{2-x}F_{1+x}$ calculated from linear fitting over 40K intervals.

2.5 Atomic Displacement Parameters

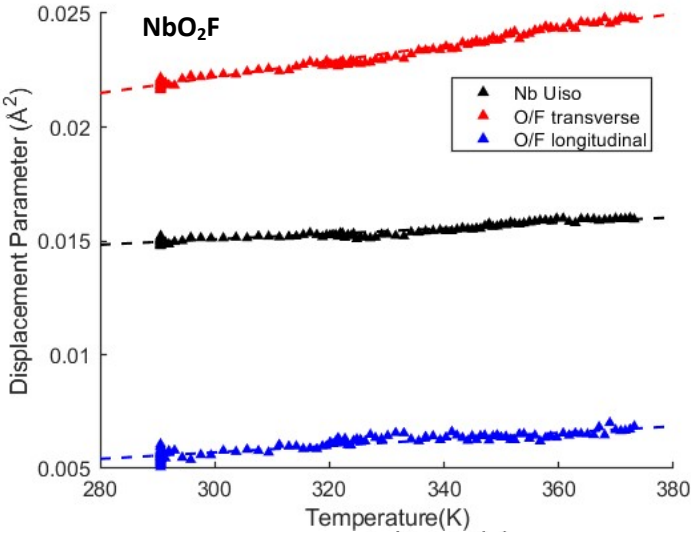

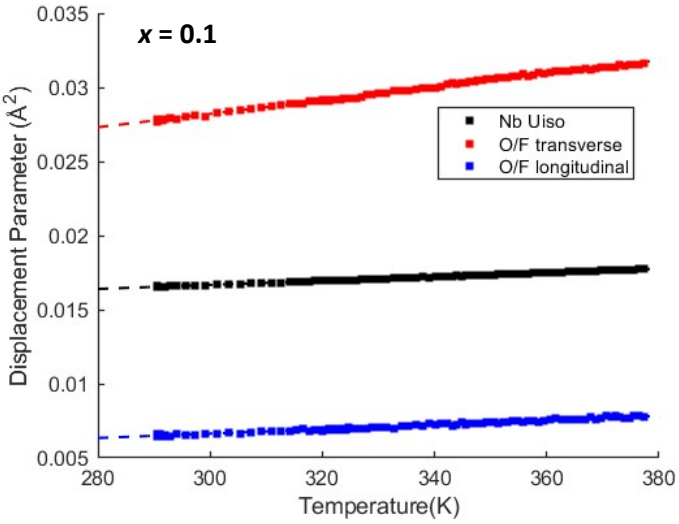

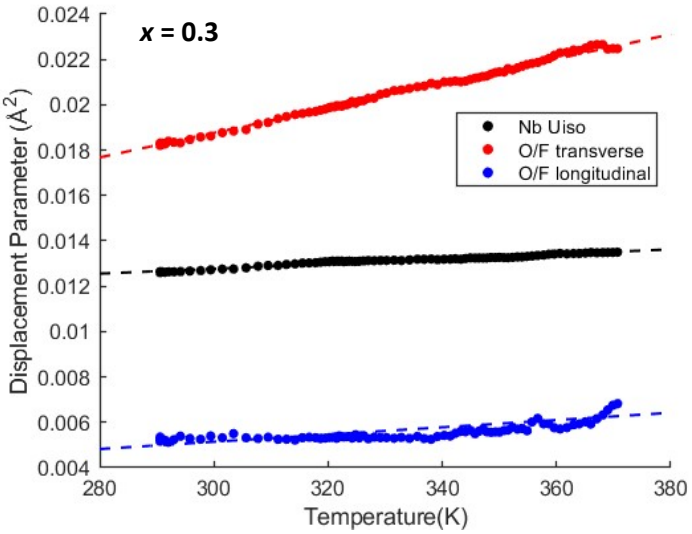

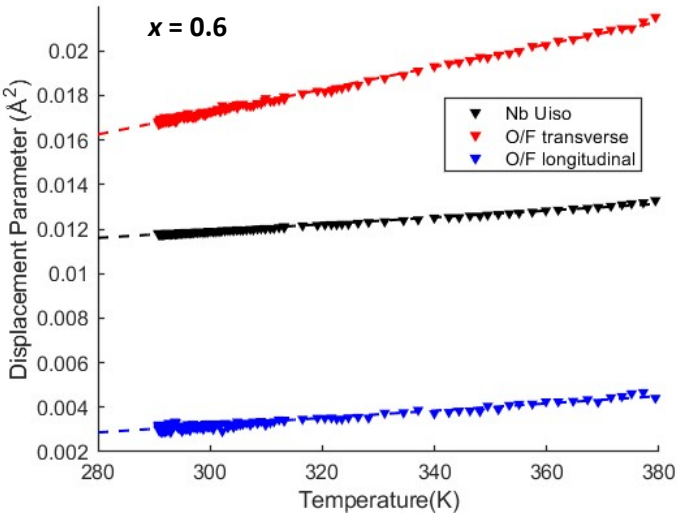

3 Magnetic Susceptibility

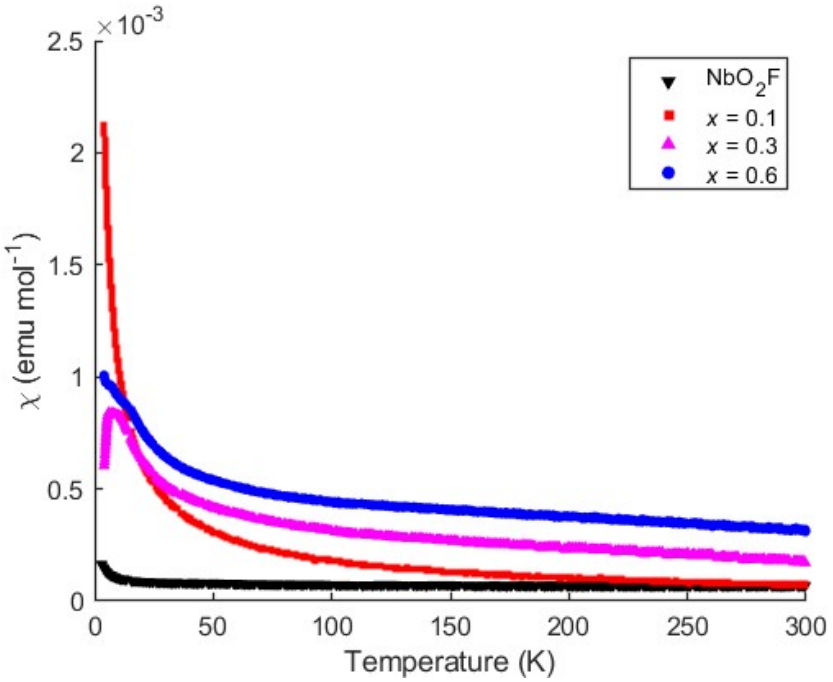

Fig. S3.1. Variation in magnetic susceptibility with temperature for $NbO_{2-x}F_{1+x}$. Only zero field cooled data is presented here as the paramagnetic region showed no difference between zero field cooled and field cooled runs. The magnetic transitions seen at low temperature are attributed to contamination caused by the synthesis procedure of the high fluorine content samples.

3.1 Magnetic Corrections

B

A

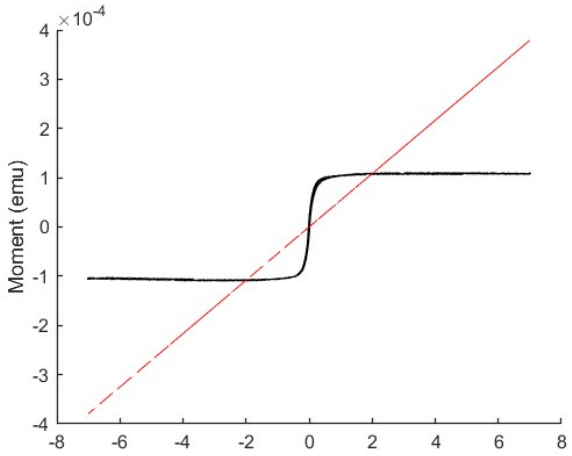

Fig. S3.2. (a) Moment against field scans for $NbO_{1.7}F_{1.3}$ at 5K and 300K showing mostly paramagnetic behaviour with a small ferromagnetic contribution (b) The 5 K moment against field scan decomposed into ferromagnetic and paramagnetic contributions.

A

B

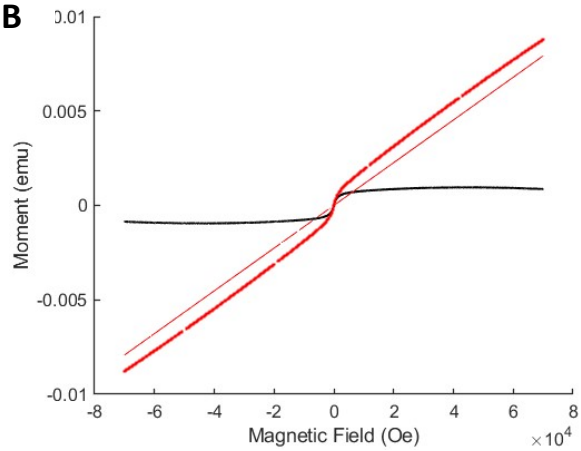

Fig. S3.3. (a) Moment against field scans for $NbO_{1.4}F_{1.6}$ at 4K and 15K showing mostly paramagnetic behaviour with a small ferromagnetic contribution (b) The 15 K moment against field scan decomposed into ferromagnetic and paramagnetic contributions.

Table 3.1 The magnitude of the corrections applied to magnetic susceptibility data on $NbO_{2-x}F_{1+x}$ before analysis. The ferromagnetic contribution was estimated from the moment-field data whilst the diamagnetic corrections were calculated from tabulated constants.[7]

Sample	**Ferromagnetic correction (10^{-4} emu)**	**Diamagnetic Correction (10^{-6} emu mol^{-1})**
NbO_2F	0	-4.210
x = 0.1	0	-4.181

x = 0.3	0.70	-4.123
x = 0.6	3.70	-4.036

3.2 Curie-Weiss Fitting

Table S3.2 Results of fitting a Curie-Weiss model (eq. 1) to magnetic susceptibility data on $NbO_{2-x}F_{1+x}$. Temperature independent corrections have been applied to the data (ferromagnetic, diamagnetic and χ_0). Fits were performed from 100-300 K.

Sample	**C (K emu mol^{-1})**	**θ_W**	**χ_0 (10^{-5} emu mol^{-1})**
x = 0.1	0.0252(11)	-40(5)	6.1(2)
x = 0.3	0.094(6)	-180.6(18)	0
x = 0.6	0.210(13)	-355(4)	0

References

1. A. P. Wilkinson, R. E. Josefsberg, L. C. Gallington, C. R. Morelock and C. M. Monaco, *J. Solid State Chem.*, 2014, **213**, 38-42.
2. F. J. Brink, L. Norén and R. L. Withers, *J. Solid State Chem.*, 2004, **177**, 2177-2182.
3. V. Dyadkin, P. Pattison, V. Dmitriev and D. Chernyshov, *Journal of Synchrotron Radiation*, 2016, **23**, 825-829.
4. K. P. Marshall, H. Emerich, C. J. McMonagle, C. A. Fuller, V. Dyadkin, D. Chernyshov and W. van Beek, *Journal of Synchrotron Radiation*, 2023, **30**, 267-272.
5. B. H. Toby and R. B. Von Dreele, *J. Appl. Crystallogr.*, 2013, **46**, 544-549.
6. K. Momma and F. Izumi, *J. Appl. Crystallogr.*, 2011, **44**, 1272-1276.
7. G. A. Bain and J. F. Berry, *J. Chem. Educ.*, 2008, **85**, 532.